Review

Israel Journal of Chemistry

DOI: 10.1002/ijch.201300128

Molecular Sensing Using Hyperpolarized Xenon NMR Spectroscopy

Krishnan K. Palaniappan,[a, b] Matthew B. Francis,[a, b] Alexander Pines,[a, b] and David E. Wemmer*[a, c]

Dedicated to the celebration of the long, consistently inventive, and productive career of our colleague and friend, Professor Shimon Vega of the Weizmann Institute of Science.

Abstract: Molecular imaging is the determination of the spatial location and concentration of specific molecules in a sample of interest. Sophisticated modern magnetic resonance imaging machines can collect NMR spectra from small-volume elements within a sample, enabling local chemical analysis. However, abundant water and fat signals limit detection of metabolites to near mM concentrations. Alternatively, targeted relaxation contrast agents enhance the relaxation of the strong water signal where they bind. A comparison of images with and without a contrast agent shows the target distribution, but high μM concentrations are needed. We have developed an approach that exploits the strong signals of hyperpolarized ^{129}Xe (an inert reporter introduced for imaging). The imaging contrast agents are composed of a biological recognition motif to localize the agent (antibodies or aptamers) and covalently tethered cryptophane cages. Xenon binds to the cryptophane and though chemical exchange saturation transfer creates contrast in a xenon image. Imaging agents can deliver many cages per target, giving detection limits in the pM concentration range. The evolution and principles of this approach are described herein.

Keywords: imaging agents · magnetic properties · natural products · NMR spectroscopy · xenon

1 Introduction

Although proton-based magnetic resonance imaging (MRI) provides a powerful modality for clinical imaging with excellent spatial resolution, it is not well suited to imaging void spaces (i.e., the lungs), low-abundance molecular markers of disease, or environments where unique proton spin densities are low. To address this limitation, hyperpolarized (hp) xenon-based NMR spectroscopy and MRI have emerged as attractive alternatives. Early studies probed xenon adsorbed to surfaces, which required hyperpolarization for sensitivity.[1] The first biological application, pulmonary void-space imaging, came in 1994 by Albert et al., who used xenon to image a mouse lung.[2] Subsequently, there have been many examples of xenon-based imaging of the lung, brain, and other tissues in both mice and humans.[3–8] Although these examples established the clinical relevance of xenon, there were still challenges associated with delivering xenon to specific locations of interest; a prerequisite for targeted molecular imaging applications. Herein, we discuss the advantages of employing xenon for molecular imaging by first describing its unique physical properties and then describing a general strategy for use in detecting specific targets of interest.

2 Physical Properties of Xenon

Xenon is a chemically inert noble gas with two NMR-active isotopes: ^{129}Xe and ^{131}Xe. The focus herein will be on ^{129}Xe, the spin $^{1}/_{2}$ isotope, which is both highly abundant (26.4% natural abundance)[9] and possesses several advantageous physical properties that make it a unique candidate for molecular imaging.[10,11]

First, xenon is soluble in many solvents, including nonpolar organic solvents, such as hexanes and benzene, as well as polar aqueous solvents, including water, aqueous buffers, and blood plasma.[12,13] Thus, xenon will uniquely partition between blood and tissue; a feature that can be utilized for specific imaging applications.[2,5,6,15] Typically the NMR spectroscopy or MRI experiments use a 2%

[a] K. K. Palaniappan, M. B. Francis, A. Pines, D. E. Wemmer
Department of Chemistry
Stanley Hall, MC-3220
University of California
Berkeley, CA 94720-3220 (USA)
e-mail: dewemmer@berkeley.edu

[b] K. K. Palaniappan, M. B. Francis, A. Pines
Materials Sciences Division
Lawrence Berkeley National Lab
Berkeley, CA 94720 (USA)

[c] D. E. Wemmer
Physical Biosciences Division
Lawrence Berkeley National Lab
Berkeley, CA 94720 (USA)

xenon gas mixture at 70–85 psi pressure in an aqueous buffer. Under these conditions, the dissolved xenon concentration is approximately 500 μM at 25 °C and 350 μM at 37 °C (using an Ostwald solubility coefficient of 0.11 at 25 °C and 0.083 at 37 °C for xenon in water).[12,13,14,15]

A major advantage of xenon is its ability to respond to very subtle changes in its local environment. Xenon possesses a large and highly polarizable electron cloud, which translates into a large chemical shift range that is sensitive to the local electronic and magnetic environment.[16] Unlike protons, which have a total chemical shift range of approximately 15 ppm, xenon exhibits a range of approximately 250 ppm, even without forming chemical bonds. It can therefore display very distinct and well-resolved chemical shifts, depending upon the solvent in which it is dissolved, or even through noncovalent association with small molecules and proteins (see Figure 1 for examples). This attribute allows for the potential to observe multiple xenon interactions at once. Additionally, ^{129}Xe NMR spectra are typically less complex than those from ^{1}H or ^{13}C NMR spectroscopy, usually showing only a few, easily interpretable signals.

Finally, ^{129}Xe is amenable to hyperpolarization; a technique that artificially modulates the spin population distribution into a nonequilibrium state.[10,17] Through a two-step process called spin-exchange optical pumping, polari-

Krishnan Palaniappan studied chemistry at Carnegie Mellon University, working in the lab of Professor Bruce Armitage, and received his B. S. degree in 2005. He then spent a year at the National Institutes of Health in Bethesda, MD, as a post-baccalaureate Fellow. Working in the lab of Dr. Kenneth Jacobson, he probed the binding sites of G-protein coupled receptors for orthogonal activation using tailored ligands. In 2006 he attended graduate school at the University of California, Berkeley, where he worked jointly with Professors Carolyn Bertozzi and Matthew Francis. His Ph.D. research included the development of chemical tools and computational strategies for identifying glycosylated proteins in complex mixtures through mass spectrometry, and the development of new xenon-based MRI contrast agents based on viral capsid frameworks for molecular imaging. In 2014 he will

Alex Pines, born in 1945, grew up in Southern Rhodesia (today Zimbabwe.) In 1962 he went to Israel where he completed his high school matriculation in agriculture and then went on to study mathematics and chemistry at the Hebrew University of Jerusalem. He obtained his B.Sc. in chemistry in 1967 and in 1968 he traveled to the USA, where he studied with J. S. Waugh at MIT, receiving a Ph.D. in chemistry in 1972. He then joined the faculty at Berkeley where he has been ever since. He was fortunate indeed to count Dr. Shimon Vega among his first post-doctoral fellows at Berkeley.

Matthew Francis was born in Ohio in 1971 and received his undergraduate degree in chemistry from Miami University in Oxford, OH, in 1994. From 1994 to 1999, he attended graduate school at Harvard University, working in the lab of Professor Eric Jacobsen. His Ph.D. research involved the development of combinatorial strategies for the discovery and optimization of new transition-metal catalysts. He then moved to UC Berkeley, where he was a post-doctoral fellow in the Miller Institute for Basic Research in Science. He worked under the guidance of Professor Jean Fréchet, focusing on the development of DNA-based methods for the assembly of polymeric materials and the application of dendrimers for drug delivery. He started his independent career in the UC Berkeley Chemistry Department in 2001, and has built a research program involving the development of new organic reactions for protein modification. These new chemical tools have been used to modify biomolecular assemblies to prepare new materials for diagnostic imaging, wastewater treatment, and solar cell development. In addition to his UC Berkeley appointment, he is also a Faculty Scientist at the Lawrence Berkeley National Laboratory.

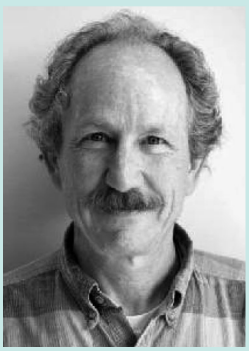

David Wemmer was born and raised in central California, obtained his B. S. from UC Davis in mathematics and chemistry (1973), then moved to UC Berkeley for graduate work in physical chemistry. Working with Alex Pines, he learned solid state and multiple quantum NMR spectroscopy methods (with large contributions from Shimon Vega), and finishing his Ph.D. in 1978. After a short post-doctoral fellowship in Dortmund, he moved to the Stanford Magnetic Resonance Lab and learned about NMR spectroscopy in biological systems; an exciting period in bioNMR because 2D methods were just being applied to protein structure determination. In 1982 he moved to the University of Washington, and applied 2D NMR spectroscopy to nucleic acids. In 1985 he returned to Berkeley. His research has continued to apply NMR spectroscopy to biological systems, but now crystallography and other methods are playing increasing roles.

Israel Journal of Chemistry

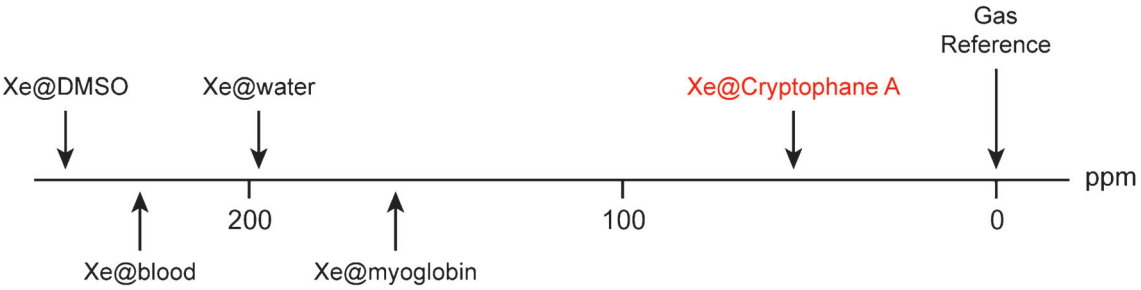

Figure 1. The chemical shift of xenon is extremely sensitive to its local environment. Examples of chemical shift values for xenon are shown in different molecular environments, including solvents, biomolecules, and synthetic molecules (e.g., cryptophane A (CryA), highlighted in red). Chemical shifts are reported referenced to xenon gas extrapolated to zero density (the 2% xenon mix generally used approximates this quite closely).

zation can be transferred from a strongly polarized alkali metal to ^{129}Xe nuclei.[18,19] In its hp state, the ^{129}Xe NMR signal can be increased by more than 10000-fold.[16,18,20] Consequently, even low concentrations of dissolved xenon can produce NMR signals comparable to that of water protons (which have a concentration of 110 M). Xenon has the additional advantage that there is no natural xenon in samples, reducing issues of background signals and dynamic range.

These favorable properties of xenon have already led to many *in vivo* imaging studies, demonstrating the biocompatibility of xenon-based MRI.[2–6] For example, hp ^{129}Xe gas was used to image the mouse lung,[2,21] the alveolar surface area in human lungs,[3] and the human chest.[4] In addition to lung imaging, tissue perfusion studies have been performed to image the rat brain[22] and the human head and brain.[4] Polarized xenon has been injected into rat tissue for rapid and localized delivery.[23] Additionally, compared with paramagnetic metals currently used as contrast agents for proton-based MRI (e.g., gadolinium), xenon has considerably lower *in vivo* toxicity.[24]

These characteristics position xenon as a powerful agent for MRI, which is sensitive to its local environment. However, unlike proton MRI, which utilizes endogenous protons in water or fat for generating images, xenon must be introduced into biological environments. After introduction to a biological system, xenon will nonspecifically partition itself into various local environments according to the strength of the interaction.[15] To utilize xenon MRI to detect specific molecules of interest, it has been necessary to develop xenon-interacting 'host molecules' that can bind xenon and report on the presence of target molecules of interest and which can also be used to enhance detection of those target molecules. The development and use of such 'adaptor' molecules are the focus of this review.

3 Detection of Xenon with Cryptophane A

Xenon can nonspecifically interact with biomolecules, including proteins and lipids, and this produces several xenon signals that occur over a modest chemical shift range when xenon is introduced into complex biological systems (cells or organisms). While this can provide some information about local composition, the xenon exchanges among many microenvironments and hence does not report specifically on the presence of any particular target of interest. To achieve specificity, 'adaptor' molecules that bind xenon and also a target of interest are necessary to achieve targeted molecular imaging.[25,26] Due to xenon's nonpolar character, a number of molecules with hydrophobic cavities have been investigated as xenon-binding hosts, including cyclodextrins, calixarenes, porous materials, hemicarcerands (including cryptophanes), and proteins.[20,25] Of these, the best-studied molecules, with respect to xenon binding, are the cryptophanes.

Cryptophanes are small, hydrophobic, cage-like molecules developed in the early 1980s by Collet and co-workers.[27,28] They consist of two cyclotriveratrylene caps and three linkers holding the caps together. A variety of cryptophane derivatives with unique xenon-binding properties have been synthesized by varying substitutions on the cyclotriveratrylene caps or the length of the linkers connecting the caps together.[28,29] Of these, cryptophane-A (CryA), which consists of methoxy-functionalized cyclotriveratrylene caps connected through three ethyl linkers, was the first of the cryptophane family of molecules to be used as a xenon-binding host for NMR spectroscopy studies (Figure 2A).[30,31] With a xenon binding affinity of approximately 4000 M^{-1} (in organic solvent)[32] and a residence time in the millisecond range (30–300 ms in aqueous solution),[32,33] CryA provides substantial xenon complexation and near-optimal exchange kinetics for NMR spectroscopy measurements.

CryA molecular cages are excellent hosts for NMR spectroscopy studies because they minimally relax xenon, while giving rise to a unique chemical shift that is well re-

Israel Journal of Chemistry

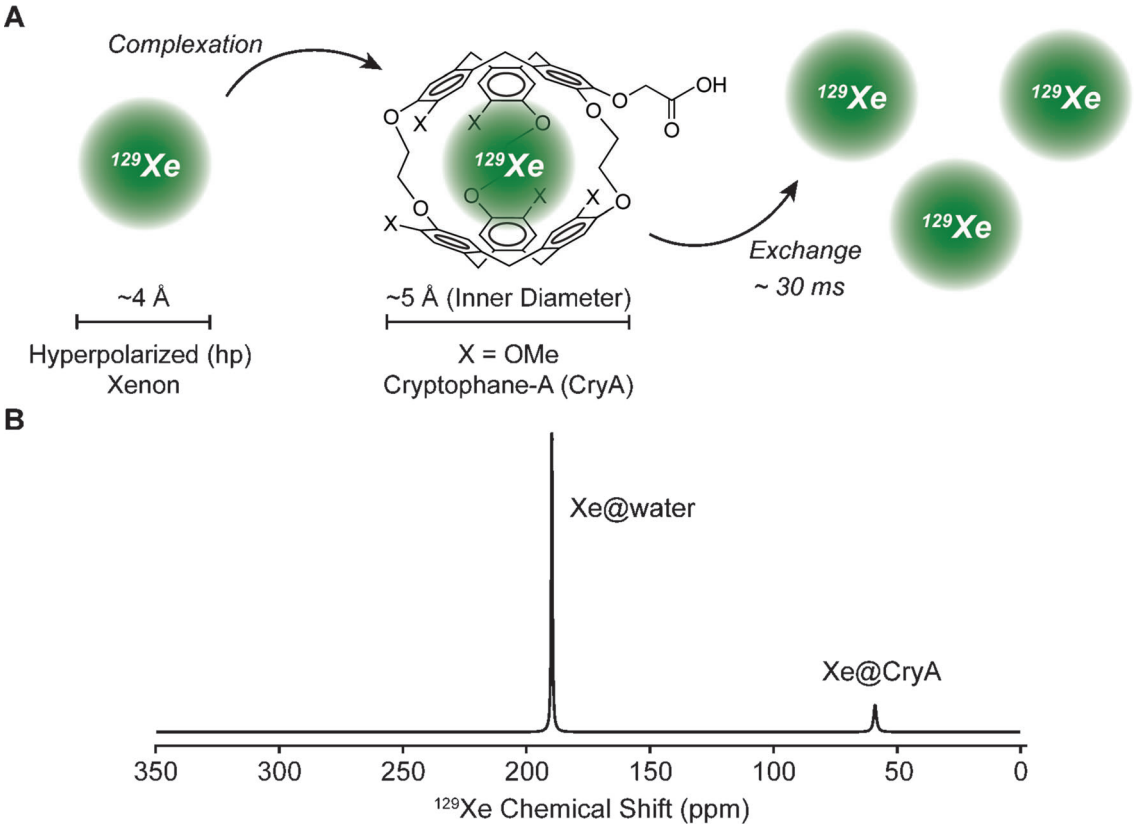

Figure 2. Direct detection of xenon through complexation with CryA molecular cages. A) The chemical structure of CryA and a schematic depiction of how it interacts with a pool of hp ^{129}Xe nuclei (depicted in green). The chemical shift of ^{129}Xe changes to approximately 60 ppm after complexation with CryA (Xe@CryA) in water. After approximately 30 ms (at room temperature), xenon will exchange with the bulk pool of free xenon in solution (i.e., Xe@water). B) A theoretical ^{129}Xe NMR spectrum of hp ^{129}Xe and CryA in water reveals two signals: one from xenon dissolved in water (Xe@water, at approximately 191 ppm) and the other from xenon bound to CryA (Xe@CryA, at approximately 60 ppm), both with reference to xenon gas (at 0 ppm). Due to the low concentration of xenon atoms in CryA, the Xe@water peak is typically much more intense than the Xe@CryA peak.

solved from that of free xenon in solution (i.e., Xe@water). Due to the highly sensitive chemical shift response of ^{129}Xe to its local environment, two distinct resonance frequencies representing the Xe@CryA and Xe@water pools can be individually detected at approximately 60 and 190 ppm downfield from the ^{129}Xe gas chemical shift (0 ppm), respectively (Figure 2B). It should be pointed out, however, that under typical conditions for NMR spectroscopy studies only a small fraction of dissolved xenon is associated with CryA in solution, since the CryA concentrations are low.[33–35] With high micromolar concentrations of CryA and moderate hyperpolarization of xenon, signals can be detected rapidly, but long acquisition times due to signal averaging are required to observe the Xe@CryA signal at lower concentrations, such as those of many targets of interest. However, high concentrations of CryA or long signal averaging are not ideal for molecular imaging applications.[35,36] An alternative method for detection, with improved sensitivity, is based on chemical exchange between the difficult to detect CryA-encapsulated xenon pool (i.e., Xe@CryA) and the easy to detect pool of free xenon in solution (i.e., Xe@water).

4 Indirect Detection of Xenon by hyperCEST

The increased sensitivity of xenon detection gained through hyperpolarization alone is insufficient to achieve the subnanomolar threshold necessary for molecular imaging applications with biological targets. One strategy to overcome this limitation is to amplify the weak signal intensity of the Xe@CryA pool by exploiting the temporary residence of xenon encapsulated in the CryA.[37]

Xenon atoms bound by CryA are in continuous exchange with the more abundant pool of dissolved xenon nuclei that are present in the surrounding aqueous environment (Figure 2A).[33,37] Interestingly, although xenon binding is fairly weak, the exchange is slow on the chemical shift timescale, but sufficiently fast that many ex-

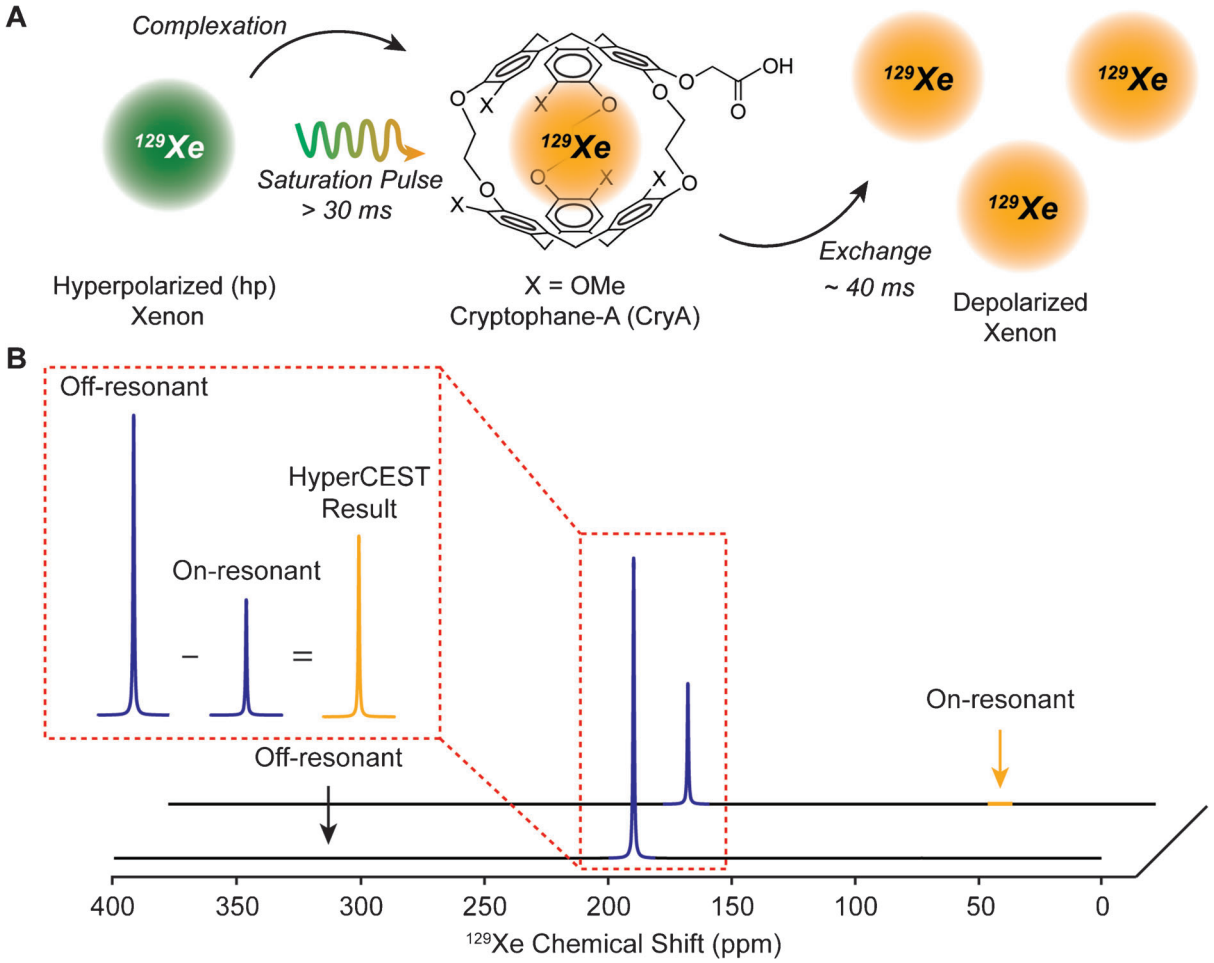

Figure 3. Sensitivity-enhanced detection of xenon using hyperCEST. A) A schematic representation of how hp ^{129}Xe (depicted in green) can be selectively depolarized (depicted in orange) when bound by CryA by applying frequency-selective RF pulses (i.e., saturation pulse). Following chemical exchange with free hp ^{129}Xe (green) from the bulk pool of xenon in solution, over time there will be an accumulation of depolarized ^{129}Xe (orange). After several cycles of selective saturation, by measuring the difference between the initial and final bulk magnetization, an indirect, but sensitive, measurement of Xe@CryA is possible. B) A schematic representation of how to measure hyperCEST contrast. HyperCEST experiments require two acquisitions to verify that a source of contrast is from CryA-encapsulated xenon: an on-resonance saturation pulse at the Xe@CryA frequency and an off-resonance pulse at a frequency equal to the separation between the Xe@water and Xe@CryA signal, but on the opposite side of the Xe@water signal. By measuring the Xe@water signal after each saturation pulse, any difference between the off- and on-resonance Xe@water signals corresponds to the presence of a Xe@CryA spin pool.

change events occur on the timescale of NMR relaxation. This property, in combination with the very distinct chemical shifts representing the Xe@CryA and Xe@water pools, serves as the basis of an indirect detection scheme through chemical exchange saturation transfer (CEST).[38] Specifically, the small Xe@CryA spin pool is saturated (i.e., depolarized) by frequency-selective radiofrequency (RF) pulses, and then these saturated spins transfer back to the bulk xenon spin pool through chemical exchange (Figure 3A). By applying RF pulses at the Xe@CryA chemical shift for a period that is long relative to the mean xenon residence time inside CryA (the inverse of the dissociation rate and greater than about 30 or 5 ms at 25 and 37 °C, respectively), the CEST mechanism allows a single CryA cage to saturate the magnetization (i.e., depolarize) of hundreds of Xe@water nuclei. Consequently, as the depolarized Xe@CryA nuclei exchange back into the bulk xenon spin pool, the intensity of the Xe@water peak will diminish. This provides a mechanism through which the RF pulses at the Xe@CryA frequency generate contrast in the Xe@water image, which can be detected much more rapidly than a direct Xe@CryA image.

The integration of CEST with hp ^{129}Xe, termed hyperCEST, was developed in 2006.[39] The complementarity of hyperpolarization and CEST arises from the fact that the bulk spin pool is typically made up of a low concentration of highly polarized ^{129}Xe spins as opposed to a high concentration of weakly polarized ^{1}H spins (for proton-based

CEST). Consequently, each xenon biosensor only has to saturate a modest number of Xe@water spins to elicit significant contrast. Furthermore, to minimize relaxation-based contrast loss, the hyperCEST detection scheme can be employed quickly relative to the long T_1 relaxation times of ^{129}Xe (approximately 4 to 10 s in oxygenated blood at 1.5 T, and 60 s in aqueous solvents at 4.7 T).[40,41]

Performing hyperCEST measurements is relatively straightforward. Following delivery of hp ^{129}Xe to the sample,[34,35] two alternating RF saturation pulses are applied, one at the Xe@CryA frequency and the other off-resonance at a frequency equal to the separation between the Xe@water and Xe@CryA signal, but on the opposite side of the Xe@water signal (to control any off-resonance effects, see Figure 3B). After each saturation pulse is applied, the Xe@water signal is recorded and then the difference between the off- and on-resonance Xe@water signals is calculated; any differences between the two signals reports directly on the presence of a Xe@CryA pool. To generate a saturation response profile (effectively a spectrum of the species being saturated), this process is repeated using different on-resonance saturation pulses (and their corresponding off-resonance pulses) and the change in the Xe@water signal is recorded as a function of the offset frequency of the RF saturation pulses applied. The presence of xenon populations exchanging with Xe@water appear as a negative peak, indicating saturation (Figure 4). For an aqueous solution containing CryA, a region of saturation centered at 60 ppm is expected. Impressively, the hyperCEST method improved the detection sensitivity of CryA-encapsulated xenon into the submicromolar to nanomolar range, without the need for long acquisition times.[39,42]

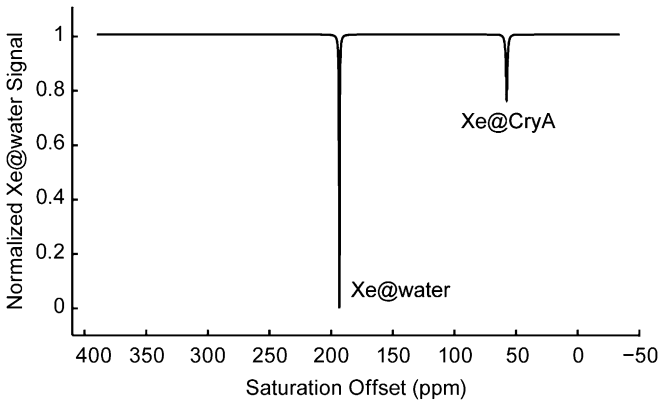

Figure 4. The hyperCEST response can be plotted as a saturation response profile. An illustration of a theoretical saturation response profile, also known as a Z-spectrum, for a solution of hp ^{129}Xe and CryA in water. Using the hyperCEST detection method, the presence of a xenon signal at a particular frequency (i.e., Xe@water or Xe@CryA) results in a negative signal, indicating saturation at that frequency.

5 Xenon Biosensors

A family of imaging agents that leverage xenon's unique physical properties and detection methods, generally called xenon biosensors, were developed for both targeted imaging and biological sensing applications.[33,37] They consist of a xenon-binding host molecule, CryA, attached to one or more biomolecules, including targeting groups for localization or substrate molecules for sensing.[43] The first demonstration of this idea was with a biotinylated CryA construct (CryA–Biotin in Figure 5) that employed a peptide linker for aqueous solubility. Interestingly, upon binding to its target substrate, streptavidin, several ^{129}Xe signals appeared in the region of the Xe@CryA chemical shift, demonstrating xenon's ability to simultaneously sense free CryA–Biotin and streptavidin-bound CryA (Figures 5B and C).[33,37] Next, several peptide-based biotinylated xenon biosensors were developed to explore the relationship between the molecular composition of a biosensor and the characteristics of its protein-bound resonances.[35,39,44] This work not only helped improve the detection of xenon biosensors, but also established their compatibility with biomolecules. Subsequently, xenon biosensors were used in a number of sensing applications, including the detection of DNA hybridization,[45] enzymatic cleavage by matrix metalloproteinase,[46] ligand binding to human carbonic anhydrase[47] and an $\alpha_{2b}\beta_3$ integrin,[48] and peptide complex formation with a major histocompatibility complex protein.[49]

The next major milestone for xenon biosensors was achieved when Dmochowski and co-workers established their cellular compatibility.[48,50] Although ^{129}Xe NMR experiments could not be performed directly with cells due to low signal sensitivity, they demonstrated cell viability after peptide-mediated uptake of crytophanes using CryA conjugated to a cell-penetrating peptide. More recently, Berthault and co-workers performed ^{129}Xe NMR measurements in the presence of live cells after targeting them with micromolar concentrations of a transferrin-functionalized biosensor.[51] That study detected biosensor binding to cells by directly measuring the Xe@CryA signal. One limitation of that approach, however, is the combination of an insensitive, direct-detection method with a biosensor displaying low binding specificity. Accordingly, to transition xenon biosensors into targeted molecular MRI contrast agents, biosensors with high specificity and high detection sensitivity at subnanomolar concentrations are necessary.

6 Signal Amplification through Scaffolding on Viral Nanoparticles

One way to improve xenon detection sensitivity beyond that achievable with the hyperCEST method alone, and to capitalize on the targeting capability of xenon biosen-

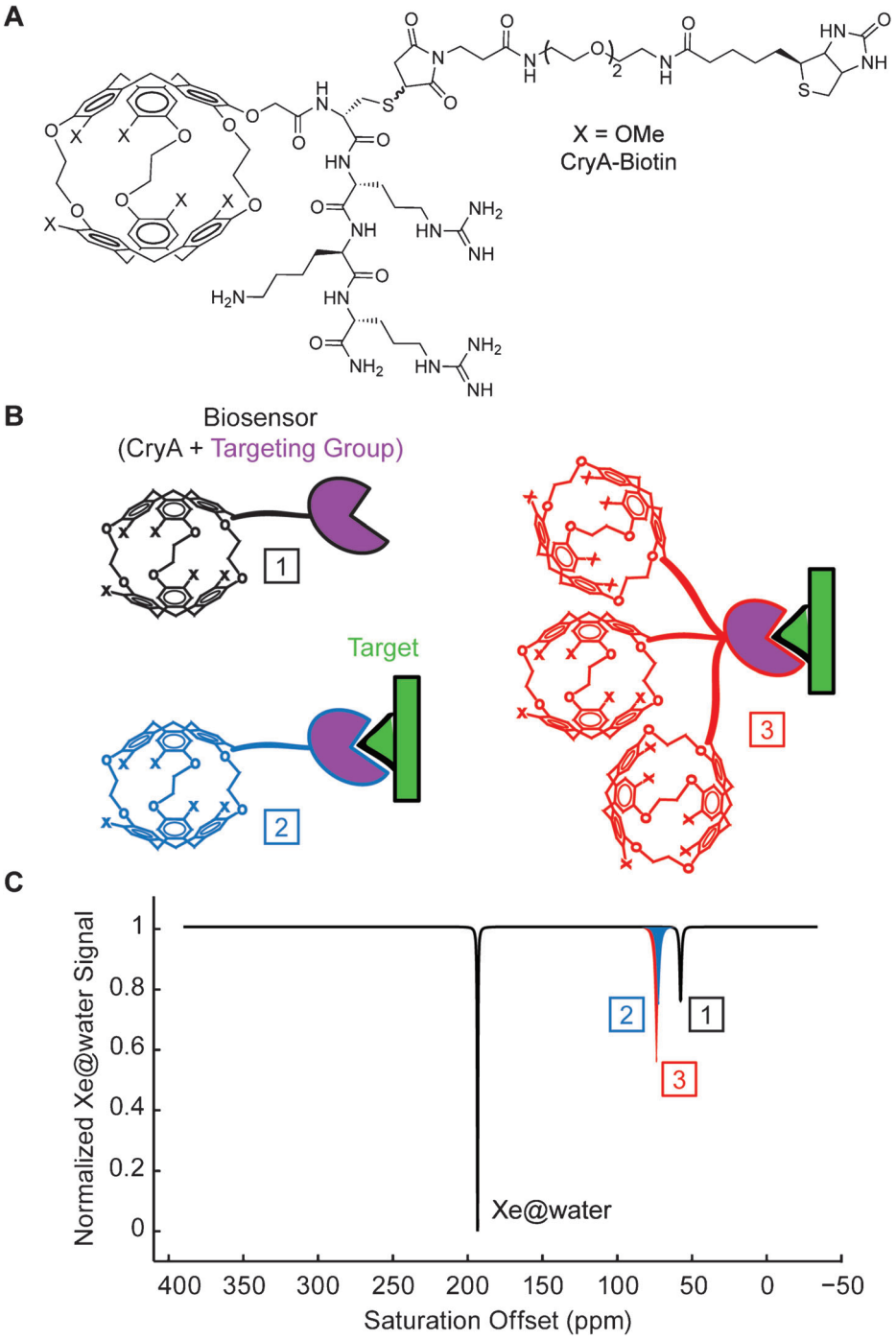

Figure 5. Xenon biosensors are targetable, sensitive, and responsive MRI contrast agents. A) The chemical structure of the first xenon biosensor (CryA–Biotin), which contained CryA, a positively charged peptide for water solubility, a polyethylene glycol linker, and a biotin group for targeting. B) Cartoons of a xenon biosensor (1), a biosensor bound to its target (2), and a multivalent biosensor bound to its target (3). C) The theoretical saturation response profiles are shown for each biosensor illustrated in B). While the signal for the biosensor alone (1) appears at a region of saturation centered at 60 ppm, after binding its target there is a slight, but resolvable frequency shift (2). A multivalent biosensor, which contains multiple CryA cages, can be employed to increase the signal sensitivity of the target-bound biosensor (3).

sors, is to turn to multivalent systems. A concept initially applied to both gadolinium- and CEST-based contrast agents for ^{1}H-based MRI,[52–60] by increasing the payload of CryA cages per biosensor molecule, a multivalent approach will enable an increased local concentration of CryA cages at the site of biosensor binding. Accordingly,

low concentrations of biosensor will correlate with much higher concentrations of CryA cages, allowing for improved detection sensitivity (Figures 5B and C, number 3).

This scaffolding concept was first demonstrated for xenon biosensors using branched dendrimers.[61] However, these polyamidoamine (PAMAM) dendrimers could only encapsulate a few CryA cages though electrostatic interactions. The low number of noncovalently bound CryA cages left room for improvement. Subsequently, both spherical and rod-like viral capsids have been used to construct targetable biosensors, where the addition of hundreds of CryA cages onto a single biomolecule resulted in constructs that were detectable by hyperCEST at subpicomolar concentrations.[62,63] Most recently, the targeting capabilities of antibodies have been combined with the multivalent scaffolding potential of the viral capsids to generate xenon biosensors that can differentiate between healthy and cancerous cell types for live-cell imaging with ^{129}Xe NMR spectroscopy.[64] Further improvements in the cryptophane cages (e.g., altering linkers between the aromatic caps) may further improve the hyperCEST signals and detection sensitivity. Reviews of some developments have been published recently.[43,65]

7 Summary and Outlook

Chemical approaches have enabled tremendous growth in molecular imaging. In the case of ^{129}Xe MRI, the combination of CryA cages combined with targeting agents to make biosensors has resulted in many successful molecular imaging and biological sensing applications. In the future, it will be exciting to apply these tools towards problems at the interface of human health and disease. In particular, many disease states are not characterized by a single biomarker, but rather a specific combination of many biomarkers. Accordingly, simultaneously visualizing multiple biomarkers *in vivo* would represent a significant achievement. Xenon's ability to respond to very subtle changes in its local environment coupled with its large chemical shift potential make it well suited for such applications.

Acknowledgments

This work was supported by the Director, Office of Science, Office of Basic Energy Sciences, Materials Sciences and Engineering Division, of the U.S. Department of Energy under contract no. DE-AC02–05CH11231 (A.P). K. K. P. was supported by a grant from the DOD Breast Cancer Research Program (BC061995). This work was taken in part from the Ph.D. dissertation of K. K. P. at U.C. Berkeley.

References

[1] D. Raftery, H. Long, H. T. Meersman, P. J. Grandinetti, L. Reven, A. Pines, *Phys. Rev. Lett.* **1991**, *66*, 584–587.
[2] M. S. Albert, G. D. Cates, B. Driehuys, W. Happer, B. Saam, C. S. Springer, Jr., A. Wishnia, *Nature* **1994**, *370*, 199–201.
[3] S. Patz, I. Muradian, M. I. Hrovat, I. C. Ruset, G. Topulos, S. D. Covrig, E. Frederick, H. Hatabu, F. W. Hersman, J. P. Butler, *Academic Radiology* **2008**, *15*, 713–727.
[4] J. P. Mugler, B. Driehuys, J. R. Brookeman, G. D. Cates, S. S. Berr, R. G. Bryant, T. M. Daniel, E. E. de Lange, J. H. Downs III, C. J. Erickson, W. Happer, D. P. Hinton, N. F. Kassel, T. Maier, C. D. Phillips, B. T. Saam, K. L. Sauer, M. E. Wagshul, *Magn. Reson. Med.* **1997**, *37*, 809–815.
[5] K. Ruppert, J. F. Mata, J. R. Brookeman, K. D. Hagspiel, J. P. Mugler III, *Magn. Reson. Med.* **2004**, *51*, 676–687.
[6] A. K. Venkatesh, A. X. Zhang, J. Mansour, L. Kubatina, C. H. Oh, G. Blasche, M. Selim Unlü, D. Balamore, F. A. Jolesz, B. B. Goldberg, M. S. Albert, *Magn. Reson. Imaging* **2003**, *21*, 773–776.
[7] D. M. Lilburn, G. E. Pavlovskaya, T. Meersmann, *J. Magn. Reson.* **2013**, *229*, 173–186.
[8] J. P. Mugler III, T. A. Altes, *J. Magn. Reson. Imaging* **2013**, *37*, 313–331.
[9] W. M. Haynes, *CRC Handbook of Chemistry and Physics*, 79th ed., CRC Press, Boca Raton, **2012**.
[10] A. M. Oros, N. J. Shah, *Phys. Med. Biol.* **2004**, *49*, R105–153.
[11] L. Schroeder, *Physica Medica* **2011**, *29*, 3–16.
[12] J. Ladefoged, A. M. Andersen, *Phys. Med. Biol.* **1967**, *12*, 353–358.
[13] H. L. Clever, *Krypton, Xenon and Radon: Gas Solubilities*, Pergamon Press, New York, **1979**.
[14] W. Kilian, F. Seifert, H. Rinneberg, *Magn. Reson. Med.* **2004**, *51*, 843–847.
[15] R. Y. Chen, F. C. Fan, S. Kim, K. M. Jan, S. Usami, S. Chien, *J. Appl. Physiol.* **1980**, *49*, 178–183.
[16] B. M. Goodson, *J. Magn. Reson.* **2002**, *155*, 157–216.
[17] A. Viale, S. Aime, *Curr. Opin. Chem. Biol.* **2010**, *14*, 90–96.
[18] T. G. Walker, W. Happer, *Rev. Mod. Phys.* **1997**, *69*, 629–642.
[19] I. C. Ruset, S. Ketel, F. W. Hersman, *Phys. Rev. Lett.* **2006**, *96*, 053002.
[20] P. Berthault, G. Huber, H. Desvaux, *Prog. Nucl. Magn. Reson. Spectrosc.* **2009**, *55*, 35–60.
[21] M. E. Wagshul, T. M. Button, H. F. Li, Z. Liang, C. S. Springer, K. Zhong, A. Wishnia, *Magn. Reson. Med.* **1996**, *36*, 183–191.
[22] S. D. Swanson, M. S. Rosen, B. W. Agranoff, K. P. Coulter, R. C. Welsh, T. E. Chupp, *Magn. Reson. Med.* **1997**, *38*, 695–698.
[23] B. M. Goodson, Y. Song, R. E. Taylor, V. D. Schepkin, K. M. Brennan, G. C. Chingas, T. F. Budinger, G. Navon, A. Pines, *Proc. Natl. Acad. Sci. USA* **1997**, *94*, 14725–14729.
[24] K. Kawakami, *Ann. Nucl. Med.* **1997**, *11*, 67–73.
[25] S. M. Rubin, M. M. Spence, I. E. Dimitrov, E. J. Ruiz, A. Pines, D. E. Wemmer, *J. Am. Chem. Soc.* **2001**, *123*, 8616–8617.
[26] C. Boutin, H. Desvaux, M. Carriere, F. Leteurtre, N. Jamin, Y. Boulard, P. Berthault, *NMR Biomed.* **2011**, *24*, 1264–1269.
[27] J. Gabard, A. Collet, *J. Chem. Soc. Chem. Commun.* **1981**, 1137–1139.
[28] T. Brotin, J. P. Dutasta, *Chem. Rev.* **2009**, *109*, 88–130.

[29] H. A. Fogarty, P. Berthault, T. Brotin, G. Huber, H. Desvaux, J. P. Dutasta, *J. Am. Chem. Soc.* **2007**, *129*, 10332–10333.
[30] K. Bartik, M. Luhmer, J.-P. Dutasta, A. Collet, J. Reisse, *J. Am. Chem. Soc.* **1998**, *120*, 784–791.
[31] T. Brotin, J. P. Dutasta, *Eur. J. Org. Chem.* **2003**, 973–984.
[32] G. Huber, T. Brotin, L. Dubois, H. Desvaux, J. P. Dutasta, P. Berthault, *J. Am. Chem. Soc.* **2006**, *128*, 6239–6246.
[33] M. M. Spence, S. M. Rubin, I. E. Dimitrov, E. J. Ruiz, D. E. Wemmer, A. Pines, S. Q. Yao, F. Tian, P. G. Schultz, *Proc. Natl. Acad. Sci. USA* **2001**, *98*, 10654–10657.
[34] S. I. Han, S. Garcia, T. J. Lowery, E. J. Ruiz, J. A. Seeley, L. Chavez, D. S. King, D. E. Wemmer, A. Pines, *Anal. Chem.* **2005**, *77*, 4008–4012.
[35] C. Hilty, T. J. Lowery, D. E. Wemmer, A. Pines, *Angew. Chem. Int. Ed.* **2005**, *45*, 70–73.
[36] T. J. Lowery, S. M. Rubin, E. J. Ruiz, M. M. Spence, N. Winssinger, P. G. Schultz, A. Pines, D. E. Wemmer, *Magn. Reson. Imaging* **2003**, *21*, 1235–1239.
[37] M. M. Spence, E. J. Ruiz, S. M. Rubin, T. J. Lowery, N. Winssinger, P. G. Schultz, D. E. Wemmer, A. Pines, *J. Am. Chem. Soc.* **2004**, *126*, 15287–15294.
[38] K. M. Ward, A. H. Aletras, R. S. Balaban, *J. Magn. Reson.* **2000**, *143*, 79–87.
[39] L. Schroder, T. J. Lowery, C. Hilty, D. E. Wemmer, A. Pines, *Science* **2006**, *314*, 446–449.
[40] A. K. Venkatesh, L. Zhao, D. Balamore, F. A. Jolesz, M. S. Albert, *NMR Biomed.* **2000**, *13*, 245–252.
[41] J. Wolber, A. Cherubini, A. S. Dzik-Jurasz, M. O. Leach, A. Bifone, *Proc. Natl. Acad. Sci. USA* **1999**, *96*, 3664–3669.
[42] L. Schroder, T. Meldrum, M. Smith, T. J. Lowery, D. E. Wemmer, A. Pines, *Phys. Rev. Lett.* **2008**, *100*, 257603.
[43] O. Taratula, I. J. Dmochowski, *Curr. Opin. Chem. Biol.* **2010**, *14*, 97–104.
[44] T. J. Lowery, S. Garcia, L. Chavez, E. J. Ruiz, T. Wu, T. Brotin, J. P. Dutasta, D. S. King, P. G. Schultz, A. Pines, D. E. Wemmer, *ChemBioChem* **2006**, *7*, 65–73.
[45] V. Roy, T. Brotin, J. P. Dutasta, M. H. Charles, T. Delair, F. Mallet, G. Huber, H. Desavux, Y. Boulard, P. Berthault, *ChemPhysChem* **2007**, *8*, 2082–2085.
[46] Q. Wei, G. K. Seward, P. A. Hill, B. Patton, I. E. Dimitrov, N. N. Kuzma, I. J. Dmochowski, *J. Am. Chem. Soc.* **2006**, *128*, 13274–13283.
[47] J. M. Chambers, P. A. Hill, J. A. Aaron, Z. Han, D. W. Christianson, N. N. Kuzma, I. J. Dmochowski, *J. Am. Chem. Soc.* **2009**, *131*, 563–569.
[48] G. K. Seward, Y. Bai, N. S. Khan, I. J. Dmochowski, *Chem. Sci.* **2011**, *2*, 1103–1110.
[49] A. Schlundt, W. Kilian, M. Beyermann, J. Sticht, S. Günther, S. Höpner, K. Falk, O. Roetzschke, L. Mitschang, C. Freund, *Angew. Chem. Int. Ed. Engl* **2009**, *48*, 4142–4145.
[50] G. K. Seward, Q. Wei, I. J. Dmochowski, *Bioconjugate Chem.* **2008**, *19*, 2129–2135.
[51] C. Boutin, A. Stopin, F. Lenda, T. Brotin, J. P. Dutasta, N. Jamin, A. Sanson, Y. Boulard, F. Leteurtre, G. Huber, A. Bogaert-Buchmann, N. Tassali, H. Desvaux, M. Carrière, P. Berthault, *Bioorg. Med. Chem.* **2011**, *19*, 4135–4143.
[52] A. Datta, J. M. Hooker, M. Botta, M. B. Francis, S. Aime, K. N. Raymond, *J. Am. Chem. Soc.* **2008**, *130*, 2546–2552.
[53] J. M. Hooker, A. Datta, M. Botta, K. N. Raymond, M. B. Francis, *Nano Lett.* **2007**, *7*, 2207–2210.
[54] O. Vasalatiy, R. D. Gerard, P. Zhao, X. Sun, A. D. Sherry *Bioconjugate Chem.* **2008**, *19*, 598–606.
[55] L. Liepold, S. Anderson, D. Willits, L. Oltrogge, J. A. Frank, T. Douglas, M. Young, *Magn. Reson. Med.* **2007**, *58*, 871–879.
[56] M. Allen, J. W. Bulte, L. Liepold, G. Basu, H. A. Zywicke, J. A. Frank, M. Young, T. Douglas, *Magn. Reson. Med.* **2005**, *54*, 807–812.
[57] E. A. Anderson, S. Isaacman, D. S. Peabody, E. Y. Wang, J. W. Canary, K. Kirshenbaum, *Nano Lett.* **2006**, *6*, 1160–1164.
[58] D. E. Prasuhn, Jr., R. M. Yeh, A. Obenaus, M. Manchester, M. G. Finn, *Chem. Commun.* **2007**, 1269–1271.
[59] P. D. Garimella, A. Datta, D. W. Romanini, K. N. Raymond, M. B. Francis, *J. Am. Chem. Soc.* **2011**, *133*, 14704–14709.
[60] S. Qazi, L. O. Liepold, M. J. Abedin, B. Johnson, P. Prevelige, J. A. Frank, T. Douglas, *Mol. Pharmaceutics* **2013**, *10*, 11–17.
[61] J. L. Mynar, T. J. Lowery, D. E. Wemmer, A. Pines, J. M. Frechet, *J. Am. Chem. Soc.* **2006**, *128*, 6334–6335.
[62] T. Meldrum, K. L. Seim, V. S. Bajaj, K. K. Palaniappan, W. Wu, M. B. Francis, D. E. Wemmer, A. Pines, *J. Am. Chem. Soc.* **2010**, *132*, 5936–5937.
[63] T. K. Stevens, K. K. Palaniappan, R. M. Ramirez, M. B. Francis, D. E. Wemmer, A. Pines, *Magn. Reson. Med.* **2012**, *69*, 1245–1252.
[64] K. K. Palaniappan, R. M. Ramirez, V. S. Bajaj, D. E. Wemmer, A. Pines, M. B. Francis *Angew. Chem. Int. Ed.* **2013**, *52*, 4849–4853.
[65] P. Berthault, G. Huber, H. Desvaux, *Prog. Nucl. Magn. Reson. Spectrosc.* **2009**, *55*, 35–60.

Received: November 2, 2013
Accepted: November 7, 2013
Published online: February 12, 2014